Impact Factor 6.1

Journal of Cyber Security

ISSN:2096-1146

Scopus

DOI

Google Scholar

More Information
www.journalcybersecurity.com

Crossref doi Google Scholar scopus

Charging of Electrical Vehicle by Using Switched Reluctance Motor Drives

A. Hima Bindu[1], G.MahaboobSubahan [2]

Assistant Professor of EEE

Department of Electrical and Electronics Engineering, Annamacharya Institute of Technology and Sciences, Rajampet

---

ABSTRACT

This paper gives a power converter geography coordinated driving and charging capacity of Switched Reluctance Motor (SRM) drive for Electric Vehicle (EV) application. In the driving mode, the transport voltage can be changed by the front-end buck converter, which meets the prerequisites of the speed open-circle and shut circle control. In addition, higher voltage demagnetization can be accomplished by associating the upper freewheeling diodes of the uneven half-span converter to the battery bank, in this way can speed up the demagnetization cycle, expand the abide point and improve the result of the engine. In battery charging mode, a bridgeless rectifier converter is developed by using two-stage windings of the SRM and the current power gadgets of coordinated power converter, without extra inductors and charging units. The battery charging and Power Factor Correction (PFC) control can be acknowledged by shut circle control of charging current.

Key Words—Integrated power converter, high voltage demagnetization, battery charger, electric vehicle, switched reluctance motor.

I. INTRODUCTION

Electric Vehicle (EV) is an effective solution for decreasing CO2 emission. Currently, EV-related technologies such as electrical motor drives design and selection, power converters topologies and control algorithms, power source and system configuration are under extensive development. Traditionally, permanent-magnet machines are preferred in EV applications owing to their highpower density and high efficiency. However, the using of large amount of rare-earth materials limits the widespread application in mass production market. As a result, developing rare-earth-free machines in EV power drive systems attracts more and more attentions. Among these, switched reluctance motor is a well-known competitive candidate in EV applications due to its robust structure, flexible control, harsh environmental sustaina- bility, excellent fault-tolerant capability, and high starting torque.

A few better SRM power converter geographies, for example, the secluded full-span converters, detached support Capacitor based converter, C-dump based converters, three-level nonpartisan point diode-braced converter, four level converters,Semi Z-source incorporated converter, double stock power converter and soon have been produced for further developing the framework functional execution.

For EV applications, the wide speed guideline capacity, over-burden maintainability, and numerous functional Capability mix present difficulties to the SRM power converter framework arrangement. The power converter ought to be used for driving the engine as well concerning charging the battery source. By and large, a minimized power converter with numerous energy change capability is profoundly required. Customarily, the unbalanced half bridge converter is used for controlling the EV SR drives. In any case, this converter can work in driving mode and regenerative slowing down mode, and along these lines an extra battery charger ought to added for charge. Also, because of the excitation and demagnetization voltages are restricted by the proper dc-interface voltage, quick excitation and demagnetization can't be accomplished. To work on the general execution of the SRM drive framework, a few high level power converters has been created for EV application. A lift front-end dc/dc converter, four-stage unbalanced half scaffold converter and buck-support PFC charger coordinated power converter is introduced in Under driving mode, the transport voltage can be very much

controlled and supported by the lift converter, and the winding put away energy can be naturally recuperated back to the battery source. For the transport voltage is consistently higher than the battery voltage, acknowledging engine speed guideline exclusively by controlling the front-end DC converter is troublesome. Furthermore, because of the demagnetization voltage is lower than the transport voltage, the quick demagnetization can't be guaranteed. In, a Miler converter with battery charging capability coordinated is proposed for module HEV, which utilizes just four power exchanging gadgets for driving and charging activity. Notwithstanding, because of the utilizing of a typical power switch in the Miler converter, the stay point ought to be limited to stay away from long demagnetization time and the negative torque effects. In a modified Miler converter with front-end dc/dc boost converter fed is constructed with two three-phase Intelligent Power Modules (IPMs). This converter can improve the high Speed operation performance and realize battery charging function with line-drawn power quality. A modular front-end circuit based multilevel converter is developed, which can provide a five-level driving control to accelerate the excitation and demagnetization processes.

However, the conduction region is restricted within 15° for the three-phase 12/8 SRM. A split power converter with flexible charging capability for afour-phase EV SRM is developed. In this converter, the central tapped winding node is utilized for connecting the phase windings with the converter circuit. In a modular tri-port converter with central-tapped node in each phase winding is proposed. In this converter, flexible energy flow control between battery, SRM and generator can be achieved, and furthermore the onboard charger for single phase or three phases AC grid can be constructed. The traditional SRM phase winding structure should be changed accordingly to construct the power converter topology. Besides, the fast demagnetization cannot be achieved. In a novel multiport bidirectional SRM drive to combine the GCU, battery, PV panel and SRM for flexible driving and charging function with fewer power devices. The dc voltage is boosted and multilevel voltage is achieved by the battery bank in the GCU driving mode, and by the charge capacitor in the pure battery driving mode. The excitation and demagnetization processes are both accelerated due to the boosted dc voltage. Besides, very flexible charging control strategies are developed. However, the bus voltage cannot be adjusted directly. In a modular multilevel converter (MMC) based switched SR drive with decentralized battery energy system is proposed, which can take advantages of the MMCs topology for SRM drives to achieve multilevel phase voltage, flexible dc-bus voltage, modular structure, and flexible control. However, many additional modular power devices and driving circuits should be added in the power converter system.An electric vehicle SR drive powered by a battery/super capacitor having grid-to-vehicle (G2V) and vehicle-to-home (V2H) and vehicle-to-grid (V2G) functions is developed. This converter is formed by a bidirectional front-end two quadrant buck/boost dc/dc converter and the SRM asymmetric bridge converter, which can ensure good acceleration/deceleration, reversible driving, and braking characteristics. In a new converter is integrated by a boost circuit, a switch capacitor with two energy storage systems, battery packs and an SRM. Many driving operation modes with boosted excitation and demagnetization voltage can be achieved. However, two battery packs or capacitors should be added in the power converter. A cascaded multiport SR drive for hybrid EV applications is proposed. This converter system can ensure flexible energy conversion among the generator/ac grid, the battery bank, and the motor, and can also achieve Battery Management (BM) function. However, to construct the front-end battery modular circuits, many additional power switches should also be added.

Generally, to develop a compact battery charger with a simple circuit and flexible control scheme is preferable for EV application. As of late, many coordinated locally available charger geographies are created for EV SR drive framework. In a buck-support PFC based battery charger is developed. In this converter, three stage windings of a four stage SRM is used, and a large portion of the power gadgets are chosen from the current driving circuit. Nonetheless, an extra power diode ought to be added. In a coordinated diode span buck-support PFC and buck PFC battery charger are created in a two IPMs based four-stage full-span converter. A basic buck-support type and buck type accusing converter of equal stage windings are created.Inthe multiport converter with multi-layered battery charging capabilities from PV, generator control unit, and ac lattice are created. In any case, the PFC capability isn't accomplished in these geographies. In a double parted converter is created for help both the dc and ac charging. While interfacing with an air conditioner power framework, the proposed geography has a value of the staggered converter, which can guarantee great PFC execution. Nonetheless, the windings ought to be splitted and the focal tapped hub ought to be remembered for the converter.

In this paper, a front-end buck dc/dc converter based EV SRM power converter with battery charging capability coordinated is proposed for accomplishing different activity modes, for example, driving activity, recovery slowing down, and battery charging. Albeit a buck front-end dc/dc converter is remotely prepared, the on-board charger is coordinated with the installed power parts and SRM stage windings. In the driving mode, the DC-transport voltage can be changed dynamically from zero to the battery voltage with the buck converter stage. Accordingly, the speed control and SRM driving control can be decoupled as the speed open-circle control and shut circle control can be executed exclusively by controlling the front-end buck converter, which might further develop the activity proficiency as the power exchanging loss of the you stage awry half extension can be brought down. Additionally, quick demagnetization can be accomplished as the

demagnetization voltage is higher than or equivalent to the DC-transport voltage, and the winding put away energy can be consequently recuperated back to the battery source during demagnetization process. In the charging mode, the power gadgets that were implanted in the SRM converter and two-stage windings are utilized to frame a coordinated bridgeless rectifier to charge the battery from the air conditioner matrix with PFC capability. Tests have been performed with a 1kW SRM model machine. The control plans of the different functional modes are appropriately planned and acknowledged in a typical ARM regulator. Detailed exploratory outcomes confirm the viability of the proposed techniques.

This paper is coordinated as follows. In Segment II and III, the proposed power converter geography and control plans of the various functional modes are introduced. Then, at that point, the exploratory outcomes are examined in Segment IV, with end made in section V.

II. TOPOLOGY AND OPERATIONAL MODES ANALYSIS OFTHE INTEGRATED POWER CONVERTER

A. Topology of the integrated power converter

The power train outline of the proposed battery-EV drive framework is displayed in Fig. 1. As contrasted and the power chart as displayed, just the one power source is utilized. The framework comprises of the battery bank, the coordinated power converter, and the SR foothold engine.

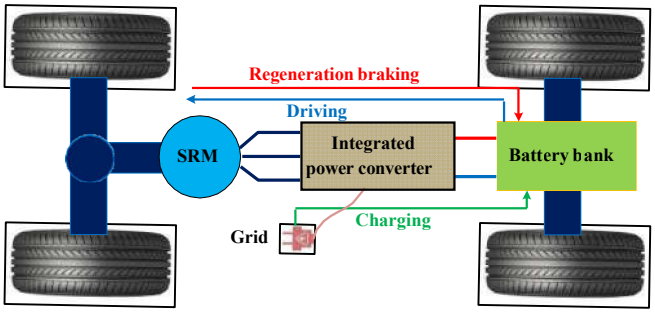

Fig. 1 The power flow of the battery-EV propulsion system.

As displayed here, the power streams of three activity modes like the engine driving mode, the regenerative slowing down mode, and the battery charging mode are completely dealt with by the proposed coordinated power converter. In SRM driving mode, the battery will supply the driving power. In the regenerative slowing down mode, portions of the slowing down energy will criticism to the battery source with the recovery control of the SRM. Furthermore, in battery charging mode, the locally available battery charger geography will be recreated without extra power gadgets, inductors and capacitors.

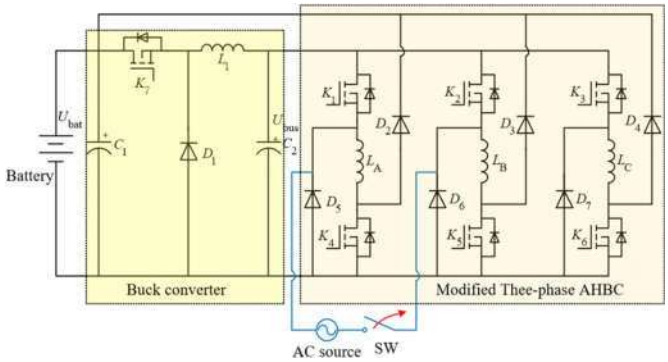

Fig. 2 Topology of the proposed integrated power converter for battery EV

SRM drive system

Fig. 2 shows the topology of the integrated power converter, which is composed of a buck front-end dc/dc converter, a modified asymmetrical half-bridge converter (MAHBC), the battery source, the SRM and the single phase AC grid connector.

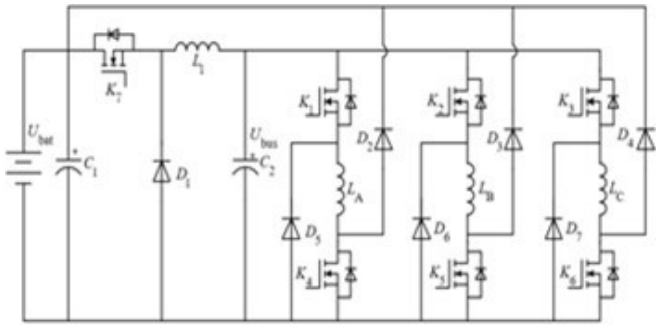

Fig.3 (a) Topology in Driving mode and regeneration braking mode

As displayed in Fig. 3(a), the buck front-end dc/dc converter is associated in series with MAHBC. In the MAHBC part, the upper freewheeling diodes are associated with the battery source straightforwardly. With this geography setup, the transport voltage of the MAHBC can be changed from zero to the battery voltage by controlling the buck converter, and the demagnetization current will input and accuse the battery straight forwardly of diminished demagnetization time length. Under regenerative slowing down mode, the battery can be charged by regenerative current straightforwardly. Besides, as displayed in Fig. 3(b), the battery charging can be accomplished by remaking a bridgeless AC-DC rectifier with the exist two power switches K4 and K5, the four freewheeling diodes D2, D3, D5 and D6, and the windings of An and B stages. As no extra power parts are included on board battery charger, the power converter has great reconciliation ability. Hence, the EV SRM power drive framework can lessen the dependence on charging stations essentially. The definite examination of the functional modes is talked about in the accompanying parts.

B. Driving Modes

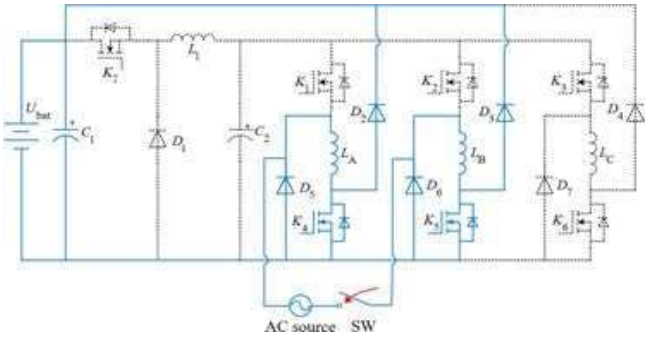

Fig. 3 (b) Topology in battery charging mode

Fig. 3 Topologies under different operation modes

Under driving mode, the battery source energy can be converted to the mechanical energy for SRM driving by the front-end buck converter and the MAHBC.

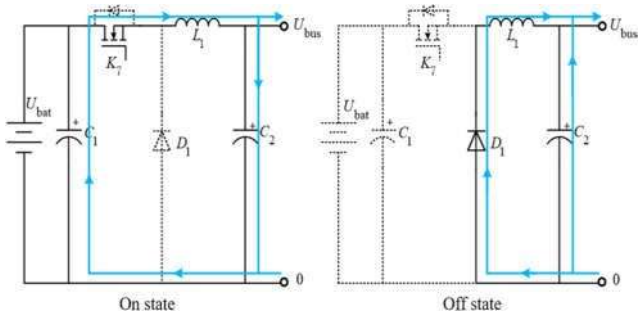

Fig. 4 The control states of the front-end buck converter

Front-end buck converter activity: By applying PWM signals in K7, the front-end buck dc/dc converter is worked for changing the transport voltage of the MAHBC. As displayed in Fig. 4, K7 is turned on to empower the inductor L1 and send the battery energy to the SRM for creating motoring force. In the off state, K7 is turned off and the energy put away in inductor L1 will be delivered to keep up with the excitation of the SRM stages. In view of volt-second equilibrium guideline, when the obligation proportion of the K7 is applied, the transport voltage can be addressed as

$U_{bus} = DU_{bat}$.

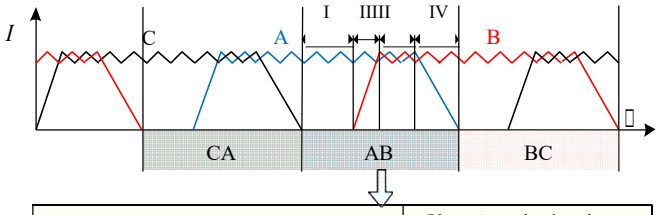

Zone I: A+, A0	Phase A conduction alone
Zone II: A+/B+, A0/B+ **Zone III:** A+/B+, A0/B+, A+/B0, A0/B0 **Zone IV:** A-/B+, A-/B0	Phase A and B conduction

Fig. 5 The control states of the SRM at different regions

MAHBC operation: Without losing consensus, stage A solitary stage conduction and stages A/B covering conduction states are chosen for examining the same circuits and the ongoing stream ways of the SRM engine activity. As displayed in Fig. 5, taking stage A and B for instance, the conduction locale is separated into four zones I to IV. In zone I, stage A is directed alone, and in different zones, A and B stage are cross-over led.

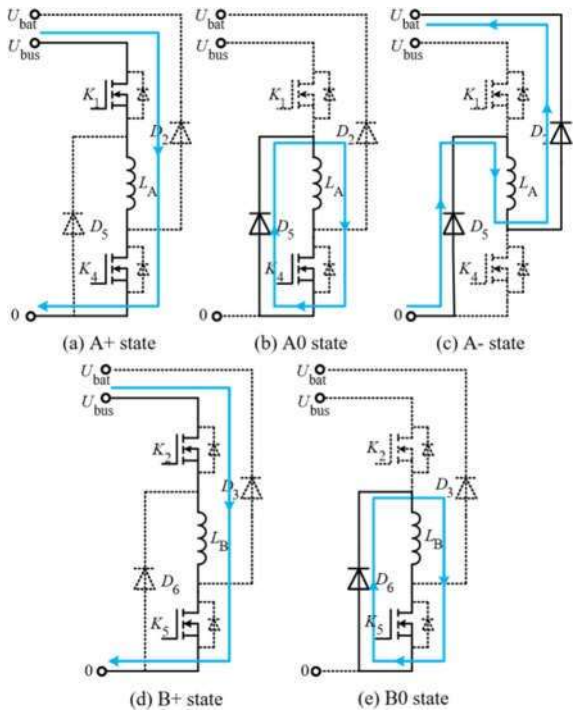

Fig. 6 The existent control states of A and B phase in the regions (a to e)

In zone I, stage A is just directed stage, which can worked under excitation mode A+ and freewheeling mode A0. The same circuits and the ongoing stream ways of A+ and A0 states are displayed in Fig. 6(a) and (b) individually. In A+ state, K1 and K4 are turned on and the transport voltage is applied in the stage winding.In A0 state, K1 is turned off and K4 is turned on, stage A will work under current freewheeling mode.As should be visible in zero voltage is applied to the stage windingand the stage current abatements as a result of the negative back electromotive drive (back EMF).

In zone II, stage B is worked under excitation mode B+. Consolidating with the activity conditions of stage A, two functional modes like A+/B+, A0/B+ are exist. The same circuits and the ongoing stream ways of A+, A0 and B+ are displayed in Fig. 6(a), (b) and (d), individually. By consolidating the same circuit of A+ and B+, the manufactured identical circuits of the activity mode A+/B+ can be formed. The manufactured comparable circuits of the activity mode A0/B+ can be created likewise.

In zone III, the stage B can work under excitation mode B+ and freewheeling mode B0, which is equivalent to that in stage A. Subsequently, consolidating the functional conditions of stage A, four functional modes like A+/B+, A0/B+, A+/B0 and A0/B0 would exist. Likewise as that in zone II, the same circuits of these four activity modes can be made by the same circuits as displayed in Fig. 6(a), (b), (d) and (e).

In zone IV, stage A is working under demagnetization mode A-. As displayed in Fig. 6(c), K1 and K4 are turned off, and the freewheeling stage current will criticism to the battery source through the two diodes D2 and D5 byJoining with the two functional methods of the stage B, two functional modes, for example, A-/B+ and A-/B0 can be created. Essentially, the same circuits of these two modes can be formed by the same circuits of A-state, B+ state and B0 state.

As displayed in Fig. 5, in the zone I to IV, there are 8 functional states in the MAHBC part, like A+, A0, A+/B+, A0/B+, A +/B0, A0/B0, A-/B+, and A-/B0. In this manner, consolidating with the on/off conditions of the front-end buck converter, there are 16 common functional states in the driving method of the proposed converter.

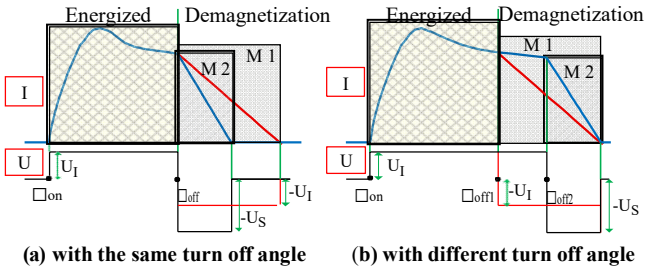

(a) with the same turn off angle **(b) with different turn off angle**

Fig. 7 **Comparison of the two control states with or without higher demagnetization voltage**

As contrasted and the conventional unbalanced half scaffold converter, the transport voltage can be changed from zero to the battery voltage, which is potential for speed guideline with the controllable transport voltage. Additionally, the demagnetization voltage is battery voltage, which is dependably higher or equivalent to the transport voltage of the MAHBC. In this way, quick demagnetization can be accomplished. As should be visible in Fig. 7(a), with higher demagnetization voltage, the stage current will diminish quicker and the negative force brought about by the demagnetization current can be brought down. Hence, it can delay the conduction locale for further developing the motoring force yield. As displayed in Fig. 7(b), the mood killer point is stretched out from θoff1 to θoff2, yet with higher demagnetization voltage applied, the demagnetization current can be diminished to zero quick, which won't fall behind when the current is decreased to focus in the conventional control strategy.

C. Regenerative Slowing down Modes

Under regenerative slowing down mode, the SRM will be controlled as a generator. As displayed in Fig. 8, the astonishing current for age can be developed by changing the excitation area [θon, θoff] of each stage. Taking stage A for instance, when the excitation signal is eliminated, the created current would freewheel through the two diodes D2 and D5 to charge the battery. The same circuits of the excitation and age modes are recorded in Fig. 8. As should be visible here, in excitation mode, both of the two power switches will be turned on to empower the stage winding. In any case, in age mode, both of the two switches will be switched off. In the slowing down mode, when the power switches of each stage are completely switched off, the stage current will freewheeling through the upper diode and criticism to the battery source.

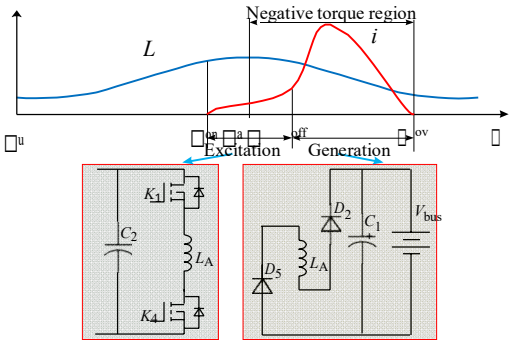

Fig. 8 Operational states under regenerative braking mode

Assuming the misfortune energy of the freewheeling circuits isn't thought of, all the slowing down energy will be input to the battery source, andhence the slowing down energy can be recovered. Furthermore, as the producing current streams in the inductance diminishing locale, negative slowing down force will be created to make the speed decline rapidly.

D. Battery Charging Mode

As displayed in Fig. 3(b), in the event that all power switches keep up with turned off with the exception of K4 and K5, the windings of An and B stages, the exist two power switches K4 and K5, the four freewheel diodes D2, D3, D5 and D6 are used for developing the bridgeless AC-DC rectifier in light of board battery charger. In this manner, no extra power gadgets ought to be added to understand the charging capability. Be that as it may, as the stage windings of two neighboring stages are chosen for utilizing as the energy-stockpiling inductors of the bridgeless rectifier, it is important to stay away from the variety of the stage inductance brought about by revolution and attractive immersion impacts.

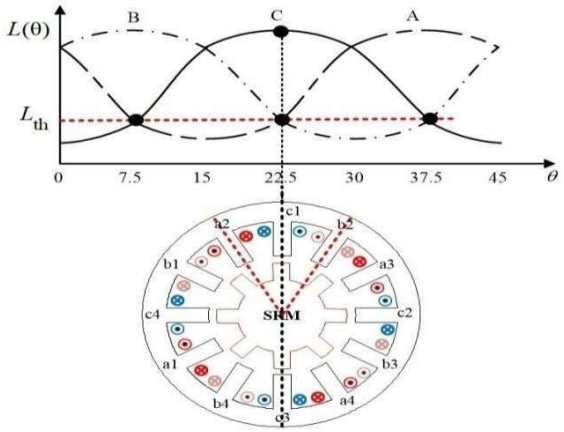

Fig.9 Lock position selection

As displayed in Fig. 9, by astonishing stage C alone, the rotor will pivot to the C-stage adjusted position, where the middle lines of the rotor shafts are lined up with the middle lines of the C-stage stator posts. Subsequently, to secure the rotor here with a mechanical installation, the winding inductance worth of stage An and B are equivalent. As should be visible in Fig. 9, their inductances are equivalent to L_{th}, which is the inductance esteem in the lower crossing point position of the three stage unsaturated inductance attributes. Moreover, in the C-stage adjusted position, both of the A and B stages are found close by their unaligned positions exclusively. Accordingly, their stage inductance will not delicate to the attractive immersions, despite the fact that there are high info flows moving through the windings.

The essential functional methods of the developed bridgeless rectifier are displayed in Fig. 10. As should be visible in Fig. 10(a) and (b), during the positive half-pattern of the air conditioner source, the dc/dc help circuit LA-K4-D2 is dynamic through diode D6, the antiparallel diode of K5, and LB. Likewise, during the negative half-pattern of the air conditioner

source, the other dc/dc support circuit LB-K5-D3 is dynamic however the diode D5, the antiparallel diode of K4, and LA., which is displayed in Fig. 10(c) and (d). The control is rearranged as the two power switches can be driven by a similar PWM signals. Moreover, Power Factor Amendment (PFC) capability can be acknowled --ged by controlling the inductors current of every half-cycle drawn from the mains and molding it like the information voltage waveform. The point by point examination of the control procedures will be talked about in Segment III.

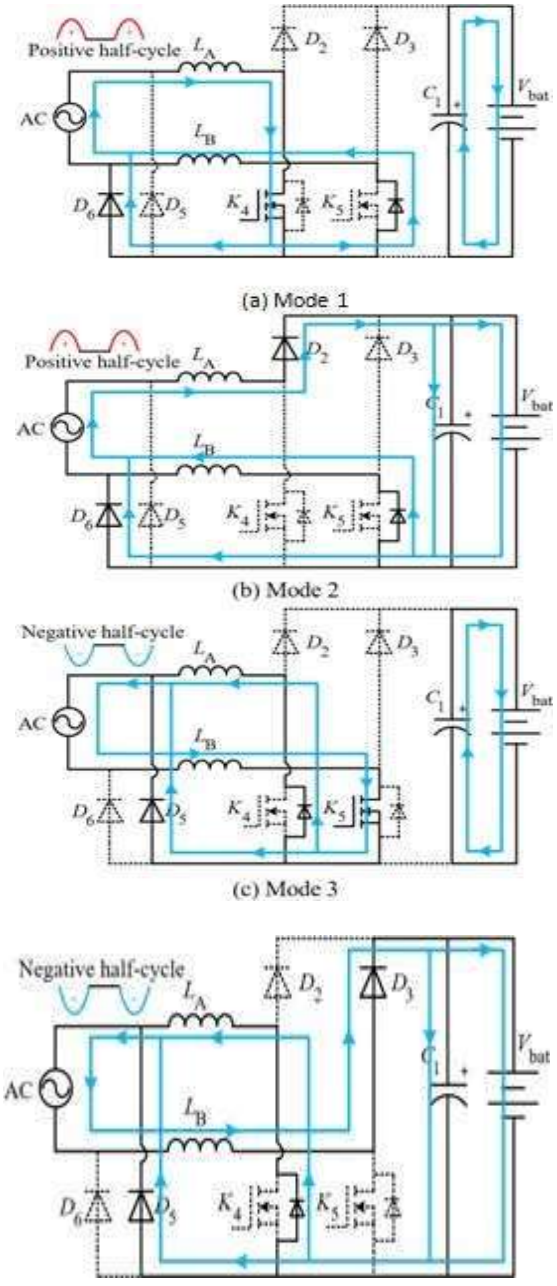

Fig. 10 Operational modes of the reconstructed bridgeless rectifier

It ought to be noticed that because of the inconsistent current in the two stages, inconsistent force would be created, which might bring about certain vibrations during the charging system. During the positive and negative half pattern of AC source voltage, separately, the all out force during the charging system isn't zero. However, by and large, for EV application, the charging power is a lot of lower than the force of the foothold engine. The allout force created during charging cycle would be tiny.

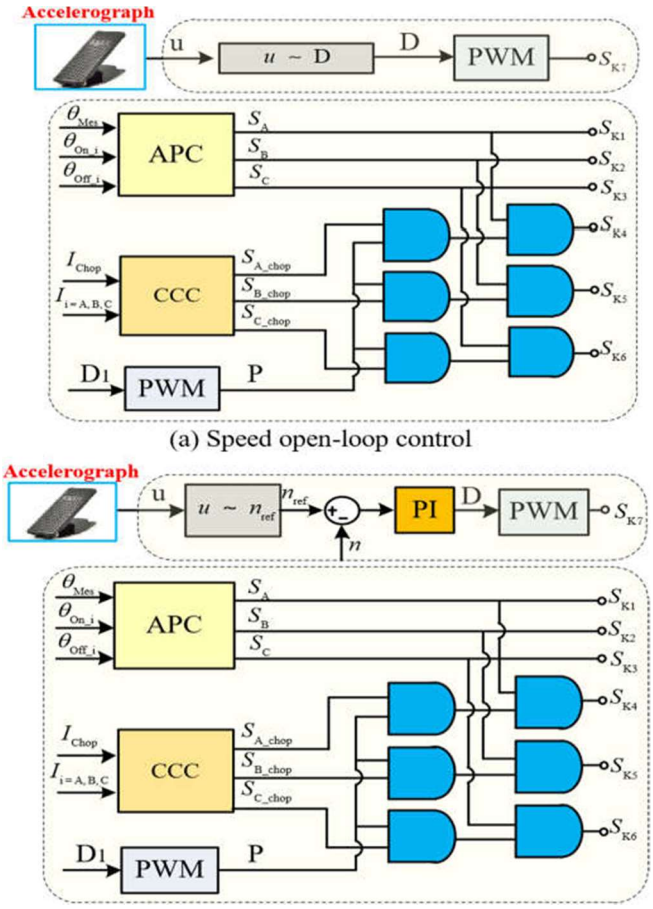

(a) Speed open-loop control

(b) Speed closed-loop control

Fig. 11 Principle diagram of the driving control strategies

CONTROLSTRATEGIES

A. Driving control strategies

As talked about in the past segment, the combination of the front-end buck converter makes the transport voltage of the MAHBC movable. Hence, it is achievable to change the rotational speed of the EV-SRM by controlling the front-end buck converter. The standard outlines of the speed open-circle and shut circle control calculations are displayed in Fig. 11(a) and (b), separately. As should be visible in Fig. 11(a), by changing over the result voltage of the EV accelerograph into the obligation proportion of the PWM control sign of the power switch K7 straightly, the front-end buckconverter can be controlled straightforwardly to yield a variable transport voltage to help the MAHBC and drive the EV-SRM. In the MAHBC part, the Conventional Current slashing Control (CCC), Angle Position Control (APC) and PWM control can be joined for creating the control signs of the six power switches K1-K6. To be noted here, just the lower switches of each stage leg are directed for producing the zero voltage freewheeling state in the conduction districts. In speed shut circle control, the result voltage of the EV accelerograph is changing over into the reference rotor speed straightly. The speed deviation is taken care of to a PI regulator to create the obligation proportion of the PWM sign of K7. Hence, the rotor speed will be controlled to follow the reference by changing the transport voltage of the MAHBC. This is the main contrast as contrasted and the open-circle control calculation. The stage recompense and current guideline control will likewise be dealt with by the MAHBC.

It ought to be noticed that the obligation proportion D1 as displayed in Fig. 11(a) and (b) can be set to 1 straightforwardly, in light of the fact that the speed control is completely dealt with by the control of the front-end converter. Consequently, the rotor speed control can be decoupled from the essential engine driving control calculation like the APC and CCC control. Nonetheless, in the customary awry half scaffold converter, the transport voltage is fixed, subsequently to change

the rotor speed, no less than one power switch of each stage leg ought to participate in the PWM guideline of the applied voltage of each stage winding. Consequently, the switch recurrence of the MAHBC will be a lot of lower than that in conventional topsy-turvy half extension converter.

B. Regenerative braking control strategy

In regenerative slowing down mode, the SRM is controlled as a generator. The control block chart is comparative as that for the speed open-circle driving control, which is displayed in Fig. 11(a). The main distinction is that the excitation locale for age energizing current development ought to be chosen close by the adjusted position. As displayed in Fig. 11(a), in this paper the excitation district is fixed at [20°, 35°] for a 12/8 construction SRM model and the obligation proportion D1 is set to 1. For this situation, the applied excitation voltage for age invigorating can be constrained by controlling the accelerograph physically.

After excitation, the creating current will input to the battery straightforwardly through the two free wheel diodes. In the interim, the negative force will created for brake.

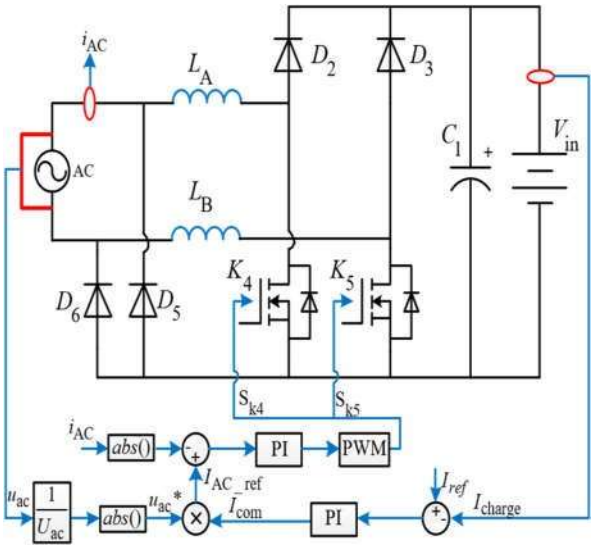

Fig.12 Principle diagram of the battery charging control strategy

C. Battery charging control strategy

Under battery charging mode, the bridgeless converter is developed as an on-board charger without adding extra power gadgets and inactive parts. In this paper, a steady typical current charging control conspire is created. As displayed in Fig. 12, the charging plan can be carried out with a twofold current circle control calculation. The external circle is the charging current criticism circle, in which a PI regulator is used for controlling the blunder between the reference current and the criticism charging current. To accomplish PFC capability, an AC input current controlled inward circle is additionally added. The AC Input Current Reference I_{AC_ref} is created by increasing outright worth of unit ac source voltage U_{ac}* with the external circle control order I_{com}. The following blunder between the I_{AC_ref} and the outright worth of the direct estimated AC input current i_{AC} is additionally managed with another PI regulator and the produced PWM signals are utilized for controlling the two power switches all the while. Through these control technique, in every half pattern of the AC period, the typical battery charging current can follow the reference current, and in the mean time the information ac current can be controlled as sinusoidal current synchronized with the AC voltage.

IV. EXPERIMENTAL RESULTS

To check the legitimacy of the proposed incorporated power converter and its control methodologies, tests have been executed in a 12/8 design SRD. The fundamental particular of the model machine is recorded in table I.

Table I
Motor specifications

Phase number	3
Stator poles	12
Rotor poles	8
Rated power	1000W
Rated Voltage	48V
Rated speed	3000rpm
Maximum phase inductance	4.52mH
Minimum phase inductance	0.56mH

As should be visible in Fig. 13, the proving ground comprises a 48V lead-corrosive battery bank, incorporated power converter, ARM based regulator, the SRM model and the dynamometer. Itemized examinations are as per the following:

Fig. 13 Experimental setup

Under driving control mode, both of the speed open-circle control and shut circle control procedures are tried. Fig. 14(a) and (b) show the fundamental stage current and voltage waveforms under APC and PWM control. In these tests, the PWM recurrence of the buck converter is set as f1=10kHz, the PWM recurrence of the MAHBC part is set as f2=6kHz, D1=1 and D1=0.5 are chosen to test the APC and PWM control of the SRM separately. As displayed in Fig. 14(a) and (b), by controlling the accelerograph, the applied voltage under conduction areas can be changed lower than the battery bank voltage, however the demagnetization voltage is fixed at the battery bank voltage. The directed inductor current waveforms of the front-end buck converter under APC and PWM control are likewise shown Fig. 14(c) and (d), separately. It very well may be seen that the control of front-end buck converter and MAHBC converter is relatively independent.These experimental outcomes are in concurrence with the essential activity capability of the proposed coordinated power converter geography. As the voltage sign of the accelerograph can be changed over completely to the PWM obligation proportion in speed open-circle control methodology, and it can likewise be utilized as a speed order for speed shut circle control. By controlling the accelerograph, the front-end buck converter can be controlled and in this way battery-bank voltage will be kicked to supply the MAHBC. In any case, in MAHBC part, the upper diode of each stage leg is associated straightforwardly to battery bank, which makes the demagnetization voltage equivalent to battery bank voltage. As the applied voltage of each stage twisting in the conduction locales is kicked and is bring down the demagnetization voltage, quick demagnetization can be guaranteed. As displayed in Fig. 14(f), with the speed shut circle regulator, the transport voltage can be changed by the front-end buck converter at various speed references, and in the mean time the rotational speed can follow the reference speed well.

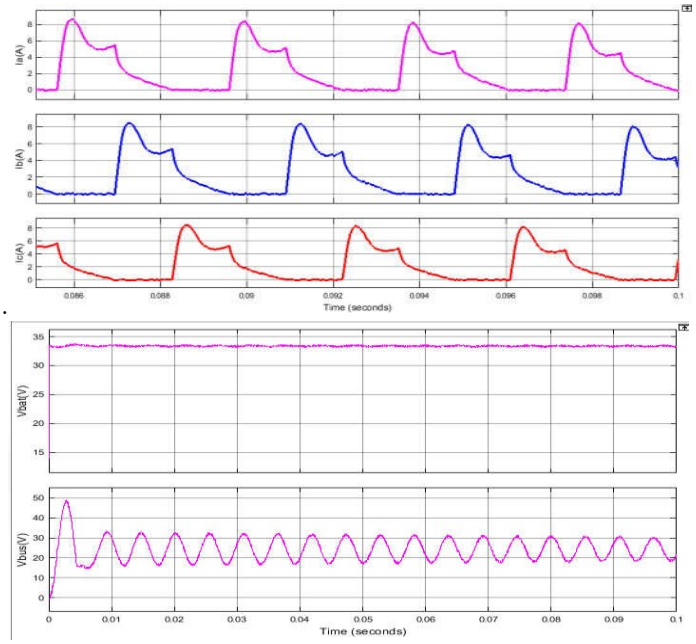

Fig 14 (a) Phase current and voltage under APC control with D1=1 and TL=0.5N.m.

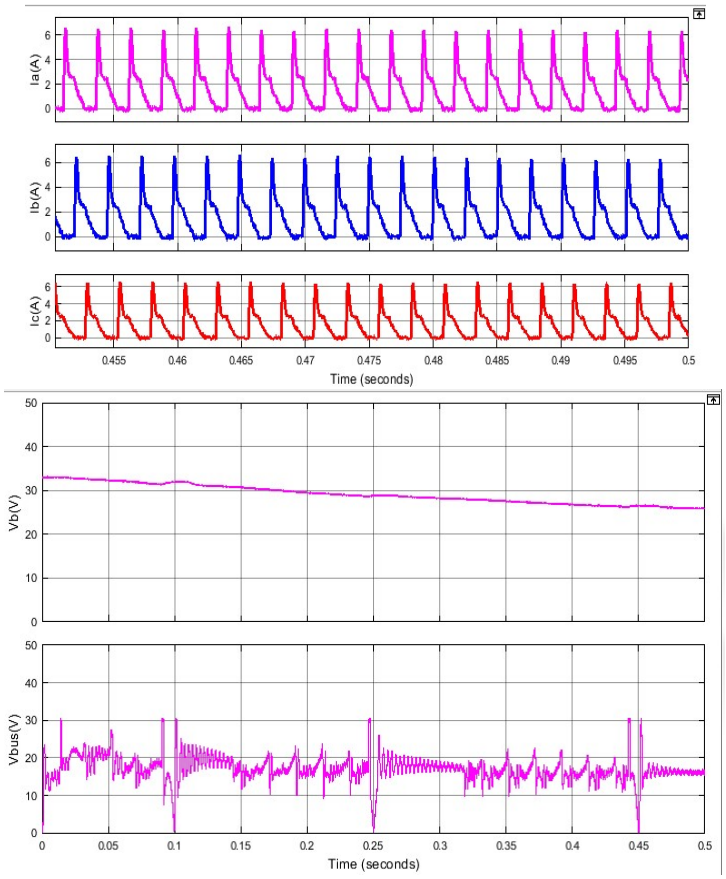

Fig. 14 (b) Phase current and voltage under PWM control with D1=0.5 and TL=0.5N.m.

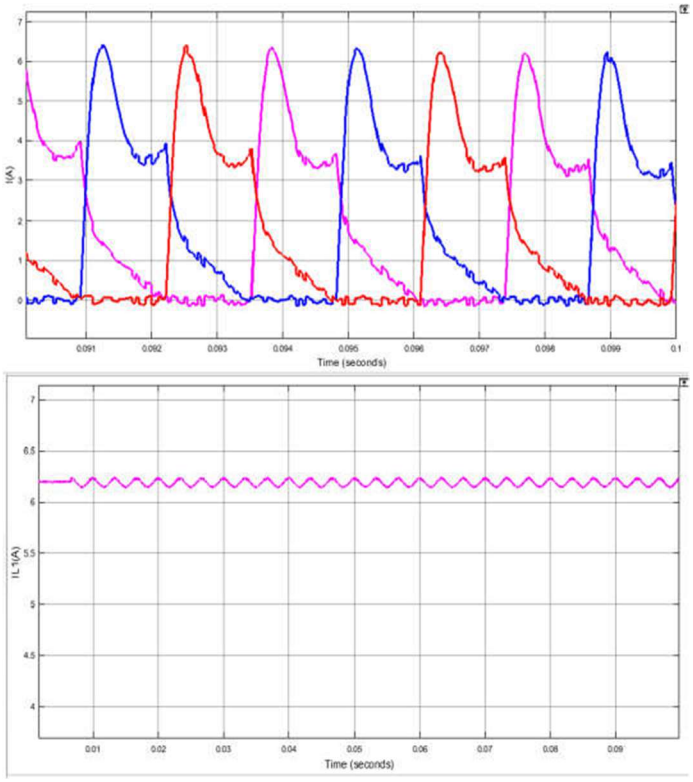

Fig. 14 (c) Phase current and inductor current under APC control with D1=1 and TL=1.5N.m.

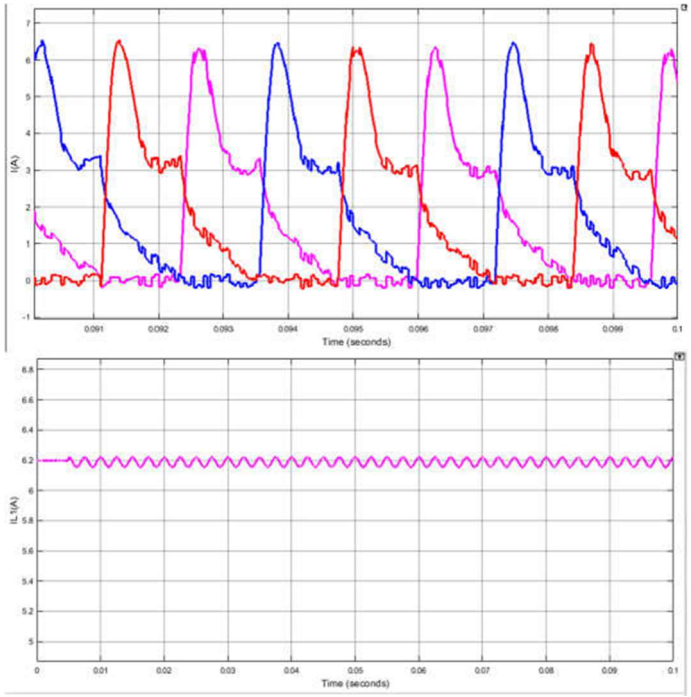

Fig. 14 (d) Phase current and inductor current under PWM control with D1=0.5 and TL=1.5N.m.

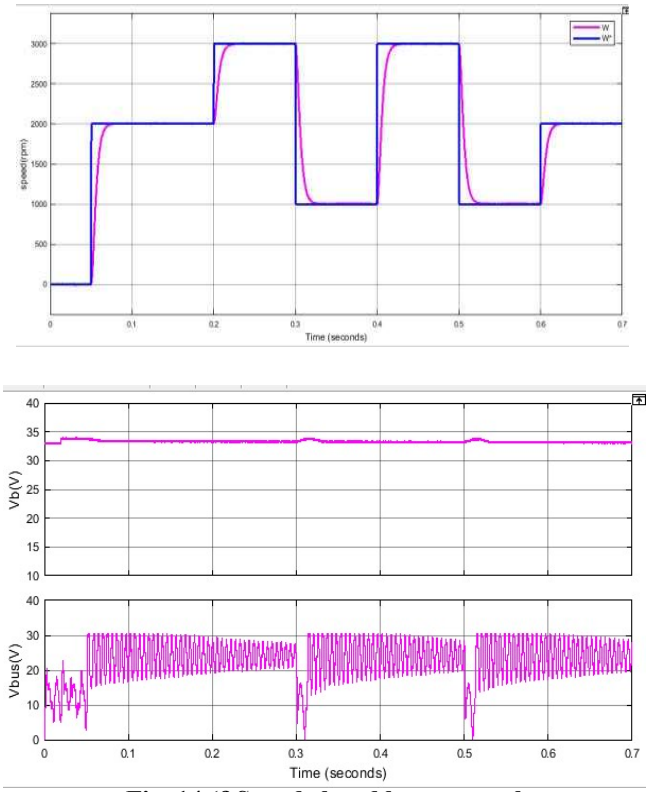

Fig. 14 (f)Speed closed loop control

Fig. 14 The Simulation results under driving control modes

In regenerative slowing down mode, the excitation district is changed to [20°, 35°] and the obligation proportion D1 is set to 1. In the excitation area, the stage winding is empowered, and when the stage is switched off, the stage will enter the age mode. The changing of stage current waveform between motoring activity and age activity should be visible in Fig. 15(a). As the generative current streams in the inductance diminishing district, negative force would be produced for slowing down, which will make the rotor speed decline quickly. It ought to be noticed that the producing current is input and charge the battery straightforwardly.

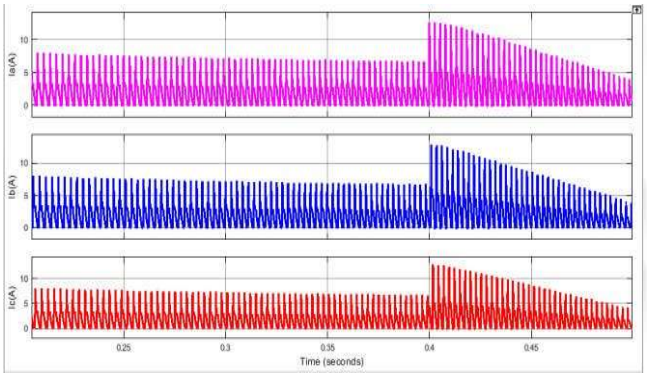

Fig. 15 (a) Dynamic change of three phase current at the transition state between driving and braking operation

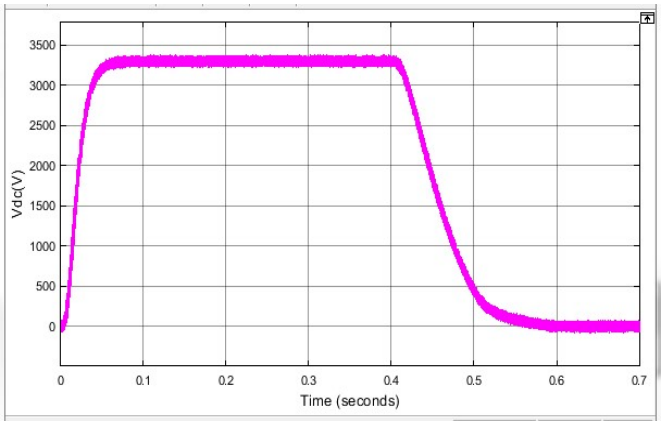

Fig. 15 (b) The change of rotor speed at different operation states

Fig. 15 The test result of the regenerative braking control

As should be visible in Fig. 15(b), the rotor speed will diminish quickly once the slowing down activity order is applied. In the test, a rotor speed limit 800r/min is set as correlation banner for eliminating the slowing down activity order. As displayed in Fig. 15(b), when the rotor speed is lower than 800r/min, the activity state is changed from regenerative slowing down activity to free-running activity. At free-running state, all exchanging signals are switched off. As contrasted and the slowing down activity express, the rotor speed is diminished a lot more slow in free-running state.

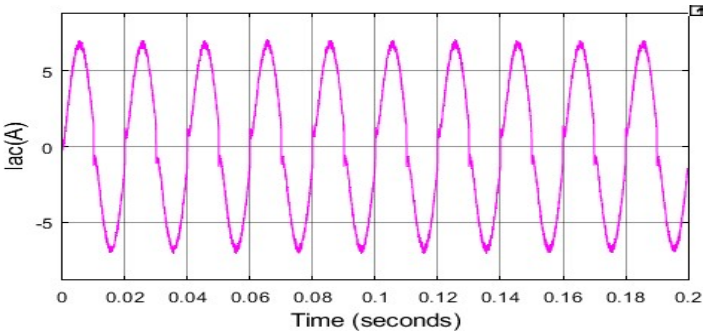

Fig. THD

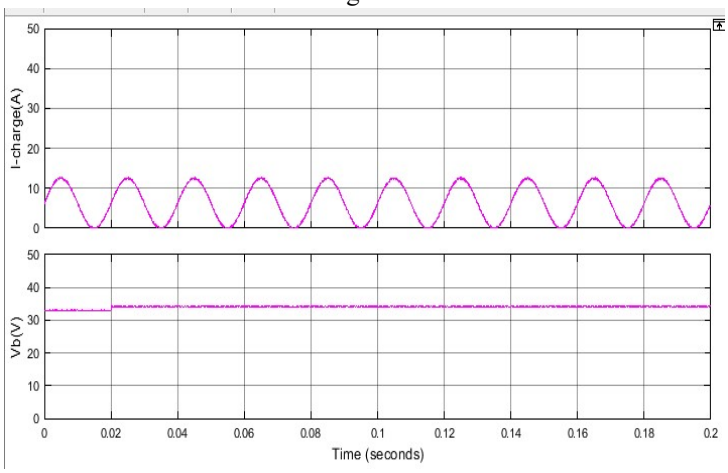

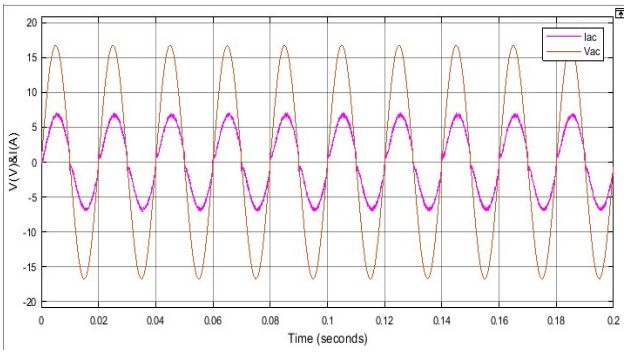

Fig. 16 The test results of the battery charging control

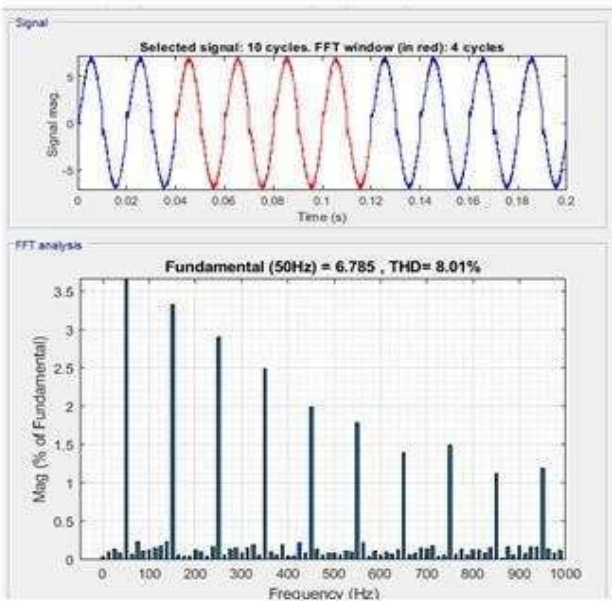

Fig. 17 FFT analysis result of the input AC current Iac

Under battery charging mode, the bridgeless rectifier is built as the on-board battery charger. To guarantee the balance of two stage windings inductance, the stage C is eager to carry the rotor to the C-stage adjusted positions. In charging mode, the SRM ought to keep halt. For the most part, to keep the rotor without pivoting, a mechanical installation ought to be utilized. However, in the event that the charging current isn't high, when the decent position is chosen, the rotor can be slowed down by setting a highload in the dynamometer. As the normal charging current in this test is just 2A, by setting a 30N.m force in the dynamometer, the SRM can be slowed down. Also, as the result voltage of the bridgeless rectifier is supported when contrasted with the air conditioner source voltage, in this way to guarantee solid 48V-battery charging, the air conditioner source voltage is brought down to 22V (RMS voltage) with the autotransformer. In the examinations, a 48V 20AH lead corrosive battery pack is utilized as the power source and the exchanging recurrence is fixed at 30kHz. As the greatest normal charging current for battery back is 3A, a 2A reference current is chosen for testing. The battery charging tests has been executed by the essential charging plan as shown in Fig. 12. As displayed in Fig. 12, the result current of the bridgeless rectifier is separated by the capacitor C1, and afterward charge the battery. As should be visible in Fig. 16, the accusing current Icharger differs of a 100Hz recurrence (two times of the air conditioner voltage). It ought to be noticed that Icharger isn't a wave current, the normal worth of which can follow the given reference current 2A. Plus, the info ac current is controlled as a sinusoidal current and is synchronized with the AC voltage.

To evaluate the PFC performance, the power factor (PF) and the Total Harmonic Distortion (THD) are analysed and measured. In theory, the power factor PF can be calculated by

$$PF = \frac{P}{\sqrt{P^2 + Q^2}}$$

Where, P is the dynamic power, Q is receptive power. In the trial, the power factor is estimated with a solitary stage electric boundary analyzer. The deliberate PF is higher than 0.99For the most part, the THD of the air conditioner source current can be determined by

$$THD = \frac{\sqrt{I_2^2 + I_3^2 + \cdots + I_n^2}}{I_1}.$$

Where, I1 is the RMS worth of the crucial current, In the RMS worth of the nth symphonious. To decide the THD, following strategies can be chosen:

1) The THD can be estimated by certain instruments like the power analyser, power quality analyser and etc..
2) The THD can be determined in the regulator online by utilizing the Fourier calculation.
3) The THD can be determined disconnected in Matlab devices utilizing the recorded current information. In this paper, the technique is chosen for deciding the THD. As displayed in Fig. 17, the THD is disconnected determined in view of the FFT examination. The determined THD with a gathering of 4 cycle current information is 8.01%.

In the trials, the charging productivity is determined by

$$\eta = \frac{I_{\text{charge}} U_{\text{bat}}}{I_{\text{ac-RMS}} U_{\text{ac-RMS}}}.$$

where, Iac-RMS and Uac-RMS are the RMS current and voltage of the input ac source.$I_{charge}$is the average charge current of the battery, U_{bat} is the battery voltage. In the test experiments, the charging efficiency reaches 0.96.

V. CONCLUSIONS

In this paper, a coordinated SRM power converter with on board battery charging capability is proposed for EV application. The comparing functional modes and control systems are explored and confirmed exhaustively with tests. The principal elements of this converter are as per the following:

1) A buck front-end dc/dc converter is incorporated with the deviated half scaffold converter, which can make the DC-transport voltage movable, and decouple the rotational speed control and the SRM driving calculation. By controlling the front-end buck converter, adaptable speed open-circle control and shut circle control can be understood. Albeit the buck converter is remotely prepared, a bridgeless rectifier in view of board charger can likewise be coordinated.

2) In driving mode, the winding put away energy can be naturally recuperated back to the battery source during demagnetization process. The demagnetization voltage is the battery voltage, which is higher than or equivalent to the DC-transport voltage, hence can guarantee quick demagnetization.

3) In battery charge mode, the on-board battery charger is framed by a bridgeless rectifier, which is developed with the implanted power gadgets and the two stage windings. All comprised parts of the chargers are put installed, and no remotely added circuit parts are required. The incorporated bridgeless rectifier can be controlled to accuse the battery of good PFC execution.It ought to be noticed that the battery charger actually has a few potential restrictions.

For example,

(1) As the bridgeless charger is a lift converter, the air conditioner source ought to be chosen in a lowerlevel voltage. In this way, for low voltage battery source application, the air conditioner matrix can't be straightforwardly utilized for charging. In any case, for high voltage battery source application, it would be more reasonable.

(2) Inconsistent prompt forces would be produced in the chose two stages, which might cause a few vibrations in the SRM during the charging system.

REFERENCES

[1] **O. C. Onar, J. Kobayashi**, and **A. Khaligh**, "A fullydirectional universal power electronic interface for EV, HEV, and PHEV applications," IEEE Trans. Power Electron., vol. 28, no. 12, pp. 5489–5498, Dec. 2013.

[2] A**. Emadi, Y. J. Lee, and K. Rajashekara**, "Power electronics and motor drives in electric, hybrid electric, and plug-in hybrid electric vehicles," IEEE Trans. Ind. Electron., vol. 55, no. 6, pp. 2237–2245, Jun. 2008.

[3] **Z.Yang, F. Shang, I. P. Brown**, and **M. Krishna- murthy**, "Comparative study of interior permanent magnet, induction, and switched reluctance motor drives for EV and HEV applications," IEEE Trans. Transp. Electrific., vol. 1, no. 3, pp. 245–254, Oct. 2015.

[4] **I. Boldea, L. N. Tutelea, L. Parsa, and D. Dorrell**"Automotive electric propulsion systems with reduced or no permanent magnets: An overview," IEEE Trans. Ind. Electron., vol. 61, no. 10, pp. 5696–5711, Oct. 2014.

[5] **E.Bostanci, M. Moallem,A. Parsapour**, and **B. Fahimi**, "Opportunities and challenges of switched reluctance motor drives for electric propulsion: A comparative study," IEEE Trans. Transp. Electrific., vol. 3, no. 1, pp. 58– 75, Mar. 2017.

[6] **A. Chiba, K. Kiyota, N. Hoshi, M. Takemoto, and S. Ogasawara**, "Development of a rare-earth-free SR motor with high torque density for hybrid vehicles," IEEE Trans. Energy Convers., vol. 30, no. 1, pp. 175– 182, Mar. 2015.

[7] **S. Song, Z. Xia, Z. Zhang**, and**W. Liu**, "Control performance analysis and improvement of a modular power converter for three-phase SRM with Y connected windings and neutral line," IEEE Trans. Ind. Electron., vol. 63, no. 10, pp. 6020–6030, Oct. 2016.

[8] **S. Song, Z. Xia, G. Fang, R. Ma**, and **W. Liu**, "Phase current reconstruction and control of 3-phase switched reluctance machine with modular power converter using single dc-link current sensor," IEEE Trans. PowerElectron., vol. 33, no. 10, pp. 8637–8649, Dec. 2017.

[9] **L. Jianing, L. Dong-Hee, X. Guoqing**, and **A. Jin-Woo**, "Analysis of passive boost power converter for three-phase SR drive,"IEEE Trans. Ind. Electron., vol. 57, no. 9, pp. 2961_2971, Sep. 2010.

[10] **A. M. Hava, V. Blasko**, and **T. A. Lipo**, "A modified C-dump converter for variable-reluctance machines," IEEE Trans. Ind. Appl., vol. 28, no. 5, pp. 1017_1022, Sep./Oct. 1992.

[11] **K. Tomczewski** and **K. Wrobel**, "Improved C-dump converter for switched reluctance motor drives," IET Power Electron., vol. 7, no. 10, pp. 2628_2635, 2014.

[12] **F. Peng, J. Ye**, and **A. Emadi**, "An asymmetric three-level neutral point diode clamped converter for switched reluctance motor drives," IEEE Trans. Power Electron., vol. 32, no. 11, pp. 8618–8631, Nov. 2017.

[13] **L. Dong-Hee** and **A. Jin-Woo**, "A Novel four-level converter and instantaneous switching angle detector for high speed SRM drive," IEEE Trans. Power Electron, vol. 22, no. 5, pp. 2034-2041, 2007.

[14] **F. Yi** and**W. Cai**, "A quasi-Z-source integrated multiport power converter as switched reluctance motor drives for capacitance reduction and widespeed-range operation," IEEE Trans. Power Electron., vol. 31, no. 11, pp. 7661–7676, Nov. 2016.

[15] **A. K. Mishra** and **B. Singh**, "Solar photovoltaic array dependent dual output Converter based water pumping using switched reluctance motor drive," IEEE Trans. Ind. Appl., vol. 53, no. 6, pp. 5615–5623, Nov./Dec. 2017.

[16] **C.Hung-Chun** and **L. Chang-Ming**, "Development of a compact switched-reluctance motor drive for EV propulsion with voltage-boosting and pfc charging capabilities," IEEE Trans. Veh. Technol., vol. 58, no. 7, pp. 3198-3215, Sep. 2009.

[17] **Y. Hu, X. Song,W. Cao**, and **B. Ji**, "New SR drive with integrated charging capacity for plug-in hybrid electric vehicles (PHEVs)," IEEE Trans. Ind.Electron., vol. 61, no. 10, pp. 5722–5731, Oct. 2014.

[18] **C. Hung-Chun** and **L. Chang-Ming**, "An integrated driving/charging switched reluctance motor drive using three-phase power module," IEEE Trans. Ind. Electron., vol. 58, no. 5, pp. 1763-1775, May 2011.

[19] **C. Gan, J. H. Wu, Y. H. Hu, S. Y. Yang, W. P. Cao**, and **J. M. Guerrero**, "New integrated multilevel converter for switched reluctance motor drives in plug-in hybrid electric vehicles with flexible energy conversion," IEEE Trans. Power Electron., vol. 32, no. 5, pp. 3754-3766, May 2017.

[20] **Y. Hu, C. Gan, S. Hu, W. Cao, X. Wang**, and **S. Finney**, "Winding-centre-tapped switched reluctance motor drive for multi-source charging in electric vehicle applications," IET Power Electron, vol. 8, no. 11, pp. 2067-2075, Nov. 2015.

[21] **Y. Hu, C. Gan, Q. Sun, P. Li, J. Wu**, and **H. Wen**, "Modular tri-port high-power converter for SRM based plug-in hybrid electrical trucks," IEEE Trans. Power Electron., vol. 33, no. 4, pp. 3247-3257, May 2017.

[22] **C. Gan, N. Jin, Q. Sun, W. Kong, Y. Hu**, and **L. M. Tolbert**, "Multiport bidirectional SRM drives for solar-assisted hybrid electric bus powertrain with flexible driving and self-charging functions," IEEE Trans. Power Electron., to be published.

[23] **C. Gan, Q. G. Sun, J. H. Wu, W. B. Kong, C.W. Shi**, and **Y. H. Hu**, "MMC-Based SRM Drives withDecentralized Battery Energy Storage System for Hybrid Electric Vehicles", IEEE Trans. Power Electron., vol. 34, no. 3, pp. 2608-2621, Mar. 2019.

[24] **K. W. Hu, P. H. Yi**, and **C. M. Liaw**, "An EV SRM drive powered by battery/supercapacitor with G2V and V2H/V2G capabilities," IEEE Trans. Ind. Electron., vol. 62, no. 8, pp. 4714-4727, Aug. 2015.

[25] **Q. G. Sun, J. H. Wu, C. Gan, J.K. Si, Y.H. Wu**, "Cascaded Multiport Converter for SRM-Based Hybrid Electrical Vehicle Applications", IEEE Trans. Power Electron., early access.